A Graph Model of the Lungs with Morphology–based Structure for Tuberculosis Type Classification

Yashin Dicente Cid[1][0000−0001−7742−5363],
Oscar Jiménez–del–Toro[1,2,3][0000−0002−0628−3764],
Pierre–Alexandre Poletti[3][0000−0001−9214−5546], and
Henning Müller[1,2][0000−0001−6800−9878]

[1] University of Applied Sciences Western Switzerland (HES–SO), Sierre, Switzerland
[2] University of Geneva, Geneva, Switzerland
[3] University Hospitals of Geneva (HUG), Geneva, Switzerland
Email: yashin.dicente@hevs.ch

Abstract. Pulmonary tuberculosis (TB) is still an important cause of death worldwide, even after being almost eradicated 40 years ago. Early identification of TB in computed tomography (CT) scans can influence therapeutical decisions, thus improving patient outcome. In this paper, a graph model of the lungs is proposed for the classification of TB types using local texture features in thorax CT scans of TB patients. Based on lung morphology, an automatic patient–specific lung field parcellation was initially computed. Local visual features were then extracted from each region and were used to build a personalized lung graph model. A new graph–based patient descriptor enables comparisons between lung graphs with a different number of nodes and edges, encoding the distribution of several node measures from graph theory. The proposed model was trained and tested on a public dataset of 1,513 CT scans of 994 TB patients. The evaluation was performed on data from a scientific challenge together with 39 participant algorithms, obtaining the best unweighted Cohen kappa coefficient of 0.24 in a 5–class setup with 505 test CTs. Even though each lung graph has a unique structure, the proposed method was able to identify key texture changes associated with the different manifestations of TB.

Keywords: Lung graph model · Texture analysis · Tuberculosis type classification

1 Introduction

Tuberculosis (TB) is a bacterial infection that remains a persistent threat and an important cause of death worldwide even after being almost eradicated around 40 years ago [21]. TB is usually clinically confined to the respiratory system, although it can spread to any organ in immunocompromised patients [4]. Medical

imaging, *i.e.* computed tomography (CT), has a major role in TB detection and associated treatment decisions, including the length of a therapy course [3]. For pulmonary TB, diagnostic imaging is particularly challenging, as the radiological signs can mimic those of other diseases, sometimes causing a delay in the start of a proper treatment strategy [15]. Moreover, early treatment can slow disease progression and reduce mortality associated with TB [2].

Since 2017, the ImageCLEF Tuberculosis challenge has been organized, promoting the development of automatic algorithms for TB type classification using a large dataset of CT scans[4]. The method proposed by Sun *et al.* trained a recurrent neural network with 2D patches and obtained the top scores in the 2017 edition of this task [19]. In 2018, Liauchuk *et al.* obtained the best scores both in unweighted Cohen kappa coefficient and overall classification accuracy [13]. They developed a lesion–based TB descriptor and trained a random forest classifier for this task. The results from both challenges show that for some TB types other algorithms obtained a higher classification accuracy, which supports the notion that there is still room for improvement [9].

Graph modeling is a complete framework that was previously proposed for brain connectivity analysis [20, 16] but has rarely been applied to other organs. Graph methods divide the brain into fixed anatomical regions and compare neural activations between regions [17]. Following a similar approach, Dicente *et al.* participated in the ImageCLEF 2017 Tuberculosis challenge [8] with a graph model of the lungs with fixed structure [5]. The approach consisted of first dividing the lung into a fixed number of regions and then creating a graph where each node represented a lung region and the edges encoded (dis)similarities between regional texture features inside the regions. During the 2017 challenge multiple combinations of pruning levels of the complete graph were tested and different similarity measures between the regional texture features [5]. In the ImageCLEF 2018 Tuberculosis challenge [9] the best model of 2017 [10] ranked second in terms of accuracy in the TB type classification task. Moreover, with the same graph model patients with pulmonary hypertension were identified, which is a very challenging task if only visual inspection of CT scans is performed [7]. Nevertheless, this graph model and all its variations were always built on a fixed initial parcellation of the lungs, *i.e.* a geometrical atlas with 36 regions.

In this work we present a new graph model of the lungs with an underlying structure derived from the morphology of the lung and not based on a geometric division. We first divide the lung volume into homogeneous regions using a generalization for 3D volumes of the SLIC (Simple Linear Iterative Clustering) algorithm [1, 18]. This technique generates a varying number of regions for each patient and therefore the graph structure differs in each patient. The graph–based descriptor of the lungs is then defined using measures from graph theory. To be able to compare the benefits of using this new lung division instead of a fixed structure to construct a graph model, we used the same regional descriptors and the same similarity measure between regions as Dicente *et al.* in [10].

[4] `https://www.imageclef.org/2017/tuberculosis`, as of 1 March 2019

We also used the same training and test dataset of the ImageCLEF 2018 TB type classification task to evaluate the outcomes.

2 Methods

This section first describes the dataset used in our experiments and then details the steps involved in the creation of this novel graph model: 1) division of the lung fields into regions; 2) extraction of local texture features in each region; and 3) construction of a lung graph encoding the comparison between the regional features of adjacent regions. Finally, the definition of a new graph–based patient descriptor is detailed.

2.1 Dataset

We used the publicly available dataset of the TB type classification task of ImageCLEF tuberculosis 2018 [9]. This dataset consists of 1,513 CT scans of 994 TB patients along with the TB type and patient age at the moment of the scan, split into 1,008 scans for training and 550 for testing. The dataset contains automatically generated masks of the lungs obtained with the method described in [6]. For each patient there are between 1 and 9 CT scans acquired at different time points. All scans of the same patient were diagnosed with the same TB type by expert radiologists. Figure 1 shows one example for each of the five TB types. Figure 2 shows examples of two patients with three CT scans each. The numbers of CT scans and patients for each TB type are shown in Table 1. Only the CT images and lung masks provided were used without using any additional meta–data *i.e.* age.

Table 1. Dataset distribution of the ImageCLEF 2018 TB type classification task. Data taken from [9].

	Num. Pats. (CT series)			
Patient set	**Train**		**Test**	
Type 1 (T1) – Infiltrative	228	(376)	89	(176)
Type 2 (T2) – Focal	210	(273)	80	(115)
Type 3 (T3) – Tuberculoma	100	(154)	60	(86)
Type 4 (T4) – Miliary	79	(106)	50	(71)
Type 5 (T5) – Fibro–cavernous	60	(99)	38	(57)
Total patients (CTs)	**677**	**(1,008)**	**317**	**(505)**

Data Preprocessing: Our approach uses rotation–invariant 3D texture descriptors that require having isometric voxels. We first made the 3D images and the lung masks isometric. After analyzing the multiple resolutions and the inter–slice distances in the dataset, we opted for a voxel size of 1 mm in all three dimension to capture a maximum of the available information.

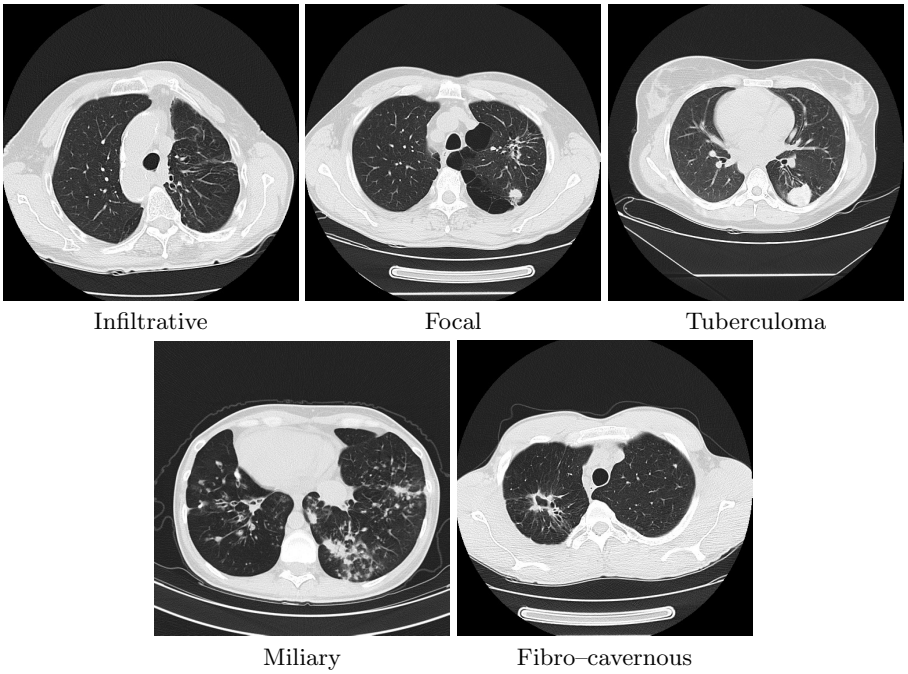

Fig. 1. CT slices of five patients from the ImageCLEF 2018 TB dataset, each one presenting a different TB type.

2.2 Lung Parcellation

Once we obtain the isometric volumes, we divide the lung area into homogeneous regions based on the HU information using a generalization for 3D volumes of the SLIC algorithm [1]. We used an initial step size s of 30 voxels (equivalent to 30 mm) followed by a refinement step where any supervoxel containing fewer than $\frac{s^3}{2}$ voxels (13,500) was merged with the most similar adjacent supervoxel. The initial step size and the refinement procedure were empirically established to obtain a reasonable number of regions with a minimum volume that can contain meaningful texture information. Figure 3 shows the supervoxelization result for one image in the dataset. The resulting lung parcellations contained between 43 and 325 regions, with an average of 170 regions per patient.

2.3 Regional 3D Texture Features

For each region r of a given lung parcellation, two texture feature descriptors were extracted: the Fourier–based histogram of oriented gradients (FHOG) [14] and the locally–oriented 3D Riesz–wavelet transform (3DRiesz) [11]. These descriptors were extracted using the same configuration as in [10] to compare to a strong baseline. FHOG was computed using 28 3D directions for the histogram, obtaining a 28–dimensional feature vector per image voxel v ($\mathbf{f}_H(v) \in \mathbb{R}^{28}$). For

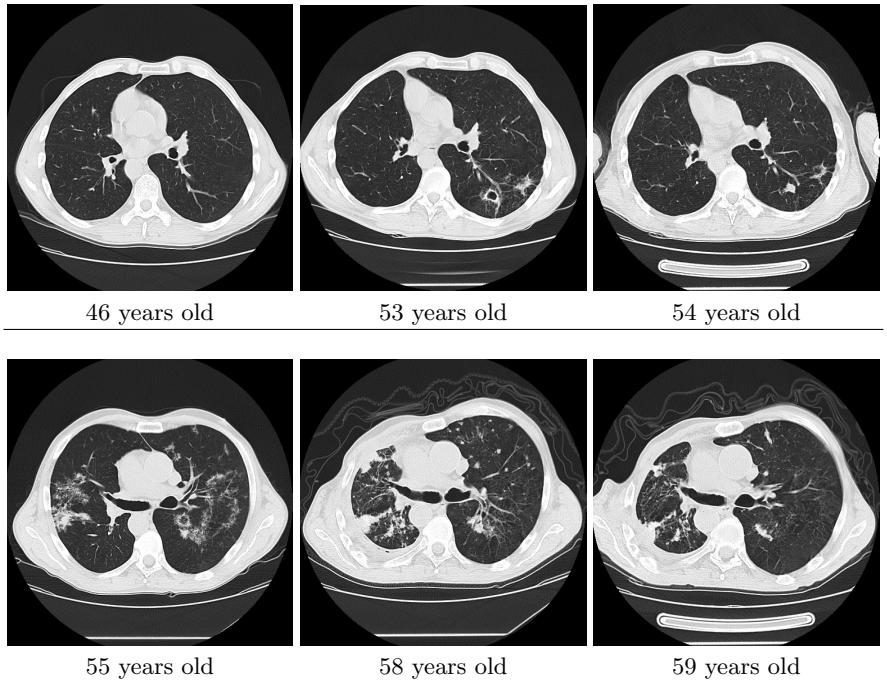

Fig. 2. Examples of two patients in the ImageCLEF 2018 TB dataset, each one with three CT scans acquired at different time points. Each row contains a slice of the three scans of a patient ordered by the patient age at the moment they were taken. The three CT images of the first row were labeled as having TB type 1 (infiltrative) while the three series in the second row are of type 4 (miliary).

3DRiesz we used the 3rd-order Riesz-wavelet transform, with 4 scales and 1st–order alignment (see [11]). The feature vector for a single voxel was defined as the absolute Riesz response along the 4 scales, obtaining a 40–dimensional feature vector ($\mathbf{f}_{\mathcal{R}}(v) \in \mathbb{R}^{40}$). Finally, the average and standard deviation of these two descriptors were obtained for each region r: $\boldsymbol{\mu}_H(r)$, $\boldsymbol{\sigma}_H(r)$, $\boldsymbol{\mu}_{\mathcal{R}}(r)$, and $\boldsymbol{\sigma}_{\mathcal{R}}(r)$.

2.4 Graph Model of the Lungs

Using the patient–specific lung parcellation defined in Section 2.2 and the regional texture descriptors detailed in Section 2.3, we create an undirected edge–weighted graph model as defined in [10]. This means: given a division of the lungs with n regions $\{r_1, \ldots, r_n\}$, we define a *graph model of the lungs* $\mathcal{G} = (\mathcal{N}, \mathcal{E})$ as a set of n nodes $\mathcal{N} = \{N_1, \ldots, N_n\}$ connected by a set of m edges $\mathcal{E}$. An undirected edge $E_{i,j}$ with associated weight $w_{i,j}$ exists between nodes N_i and N_j if regions r_i and r_j are 3D adjacent in the lung parcellation. The weight $w_{i,j}$ is defined as the correlation distance between the regional feature vectors. Figure 4 contains a 3D visualization of the graph using the patient–specific lung parcellation.

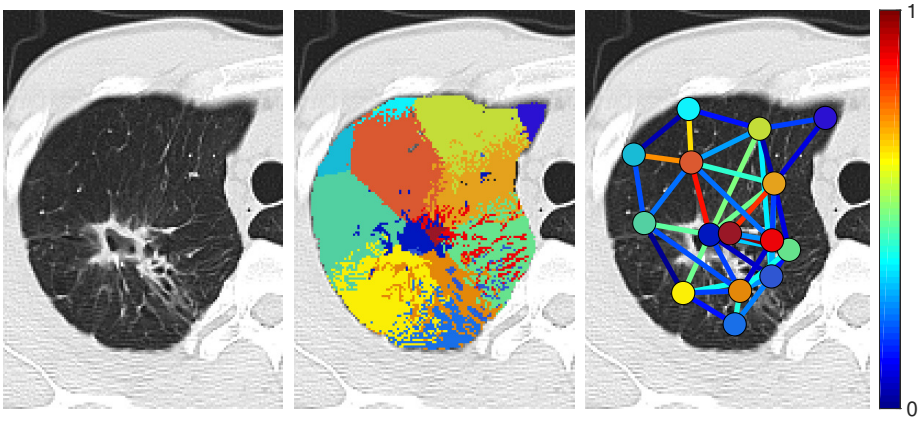

Fig. 3. From left to right: Cropped CT slice of a patient with fibro–cavernous TB shown in Figure 1, the automatically generated supervoxelization (or lung parcellation) and the subgraph containing the nodes that correspond to the regions present in the cropped CT slice. This subgraph contains 25 nodes and 42 edges, whereas the full graph of this patient contained 233 nodes and 2,035 edges (see Figure 4). The color of the nodes matches the color of the region that they represent. The edges are colored according to their weight and are normalized between 0 and 1. For this example we used as weight the correlation distance between the average absolute Riesz response in each region $\boldsymbol{\mu}_H(r)$ (see Section 2.3).

2.5 Graph–based Patient Descriptor

Dicente *et al.* defined in [10] a graph model of the lungs containing the same number of nodes and the same edges for all patients. Therefore, a graph–based patient descriptor $\boldsymbol{w}_p$ was defined as the collection of weights in the graph, sorted with respect to their position in the adjacency matrix. Our graph model of the lungs on the other hand contains a varying number of nodes (and edges) for each patient and the above mentioned approach can not be used. We described each graph with a fixed number of graph measures in order to compare graphs of different patients.

For each node N in the graph $\mathcal{G}$ we computed five graph centrality measures: the weighted degree $d^w(N)$, the relative weighted degree $d^r(N) = \frac{d^w(N)}{d(N)}$ (the weighted degree divided by the degree), the weighted closeness $c^w(N)$, the relative weighted closeness $c^r(N) = \frac{c^w(N)}{d(N)}$ (the weighted closeness divided by the degree) and the weighted betweenness $b^w(N)$. Each of these measures provided different information about the importance of each node inside the graph (see Figure 5). Considering the entire set of nodes $\mathcal{N}$ in $\mathcal{G}$, each of these five measures results in a distribution: $D^w_{\mathcal{G}} = \{d^w(N)\}$, $D^r_{\mathcal{G}} = \{d^r(N)\}$, $C^w_{\mathcal{G}} = \{c^w(N)\}$, $C^r_{\mathcal{G}} = \{c^r(N)\}$ and $B^w_{\mathcal{G}} = \{b^w(N)\}$, where $N \in \mathcal{N}$. Then, we described each of these distributions using 10 equidistant percentiles from 0 to 100 (step size of $11.\overline{1}$), with percentiles 0 ($\pi_1(X)$) and 100 ($\pi_{10}(X)$) being the minimum and max-

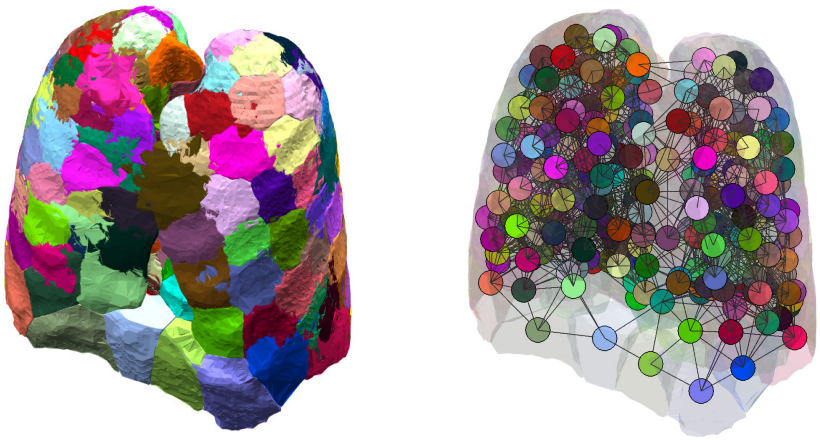

Lung parcellation Lung graph

Fig. 4. Morphology–based lung parcellation and graph derived from it. Each region is identified by a node and the edges are defined between nodes of 3D–adjacent regions in the lung parcellation. The color of the nodes corresponds to the color of the lung region that they represent.

imum values in the distribution, respectively. Let $\boldsymbol{\pi}(X) = (\pi_1(X), \ldots, \pi_{10}(X))$ be the vector composed of the 10 percentiles $\pi_k(X)$ of a distribution X. Our graph–based patient descriptor is then defined as:

$$\boldsymbol{\omega}(\mathcal{G}) = (\mu_w, \boldsymbol{\pi}(D^w_{\mathcal{G}}), \boldsymbol{\pi}(D^r_{\mathcal{G}}), \boldsymbol{\pi}(C^w_{\mathcal{G}}), \boldsymbol{\pi}(C^r_{\mathcal{G}}), \boldsymbol{\pi}(B^w_{\mathcal{G}}))$$

where μ_w is the mean of the weights in the graph.

For each patient p with graph model $\mathcal{G}_p$, its graph–based patient descriptor $\boldsymbol{\omega}(\mathcal{G}_p)$ belongs to $\mathbb{R}^{51}$. From now on, $\boldsymbol{\omega}(\mathcal{G}_p)$ is referred to as $\boldsymbol{\omega}_{\mathbf{f},p}$, where $\mathbf{f}$ corresponds to the regional feature used to build the graph $\mathcal{G}_p$.

Concatenation of Patient Descriptors: As mentioned in Section 2.3, four regional features were computed in each region of the lung parcellation ($\boldsymbol{\mu}_H(r)$, $\boldsymbol{\sigma}_H(r)$, $\boldsymbol{\mu}_{\mathcal{R}}(r)$, and $\boldsymbol{\sigma}_{\mathcal{R}}(r)$) providing complementary information about the texture and its variability. Given a patient p, a different weighted graph (same nodes and edges but different weights) was obtained from each of these textural features. The final patient descriptor $\hat{\boldsymbol{\omega}}_p$ used in our experiments was defined as the concatenation of the four graph–based patient descriptors:

$$\hat{\boldsymbol{\omega}}_p = (\boldsymbol{\omega}_{\boldsymbol{\mu}_H,p}, \boldsymbol{\omega}_{\boldsymbol{\sigma}_H,p}, \boldsymbol{\omega}_{\boldsymbol{\mu}_{\mathcal{R}},p}, \boldsymbol{\omega}_{\boldsymbol{\sigma}_{\mathcal{R}},p}) \in \mathbb{R}^{204}.$$

3 Experimental Setup

We applied Z–score normalization to each dimension of the descriptor vectors $\hat{\boldsymbol{\omega}}_p$ using the mean and standard deviation computed on the training set vectors.

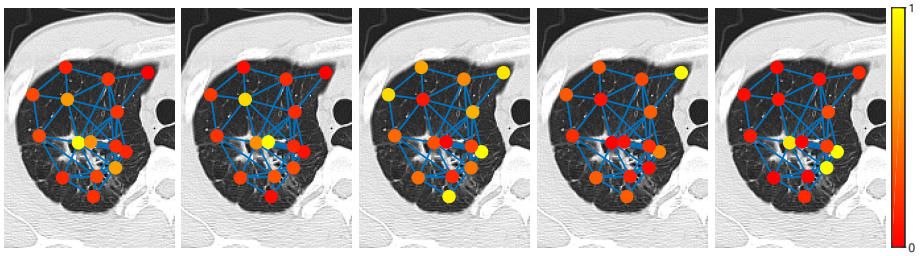

Fig. 5. Visualization of the distribution along the graph shown in Figure 3 of the five graph measures extracted in each node of the graph. From left to right: Weighted degree D^w, relative weighted degree D^r, weighted closeness C^w, relative weighted closeness C^r and weighted betweenness B^w. For better visualization, the values of each measure are normalized between 0 and 1 considering only the values in the nodes present in the depicted slice.

Then, we used linear discriminant analysis (LDA) as a dimensionality reduction technique and as a classifier algorithm in a 5–class setup. The optimization of the LDA classifier was done using 10–fold cross–validation with random sampling without repetition and grid search over the parameter space.

The ImageCLEF TB dataset contained more than one CT scan for several patients (see Section 2.1). In our experiments we treated each CT scan as a different instance. However, since the evaluation by the ImageCLEF organizers was done at a patient level, we combined the predictions of the CT images of each patient to obtain a final predicted class per patient. This combination was obtained by averaging the probabilities of the LDA classifier. The final evaluation on the test set was done by the ImageCLEF organizers using the same measures as the ones reported during the challenge: the unweighted Cohen kappa coefficient and the accuracy. Moreover, the true positive rate (TPR) of each class was provided.

4 Results

Table 2 shows the results obtained by our approach and by the top three groups that participated in the ImageCLEF 2018 TB type classification task: the *UIIP_BioMed* [13], the *fau_ml4cv* [12] and the *MedGIFT* [10] groups. All results were provided by the ImageCLEF 2018 TB organizers. The approach of Dicente *et al.* participated as the MedGIFT group. The results obtained by our new graph model are much higher than the ones obtained by the MedGIFT group using a related approach and slightly higher than the winner of the challenge in terms of Cohen's kappa. Figure 6 contains the confusion matrix of our approach and Figure 7 shows the true positive rate (TPR) of our approach and the 3 best participants.

Table 2. Results obtained by our approach and by the 3 best participants in the ImageCLEF 2018 TB type classification task.

Group name	Kappa	Accuracy
Our approach	**0.2385**	0.4196
UIIP_BioMed [13]	0.2312	**0.4227**
fau_ml4cv [12]	0.1736	0.3533
MedGIFT [10]	0.1706	0.3849

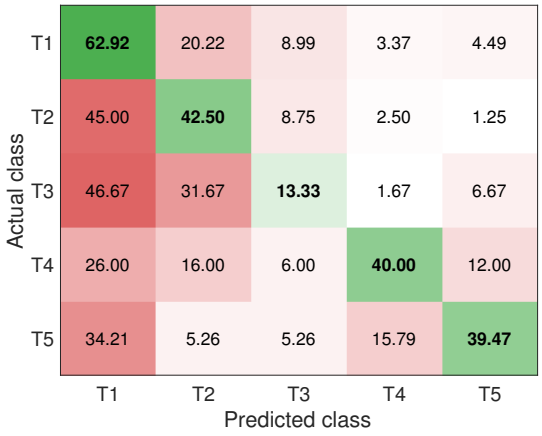

Fig. 6. Confusion matrix of our approach in %.

5 Discussion

In this work we used a graph model with an underlying structure that it is based on the morphology of the lungs. The comparison between graphs of different patients was then translated to the comparison of the distributions along each graph for five graph measures, extracted in each node. The selected node measures are both local (considering only the weights of incident edges to a given node) and global (considering the whole structure of the graph). In Figure 5, it can be seen how the selected node measures are complementary and each of them highlights different but relevant nodes. The manual analysis of several graphs revealed that the distributions of these measures usually did not follow a normal distribution and therefore the use of central moment statistics was not appropriate. The use of percentiles as distribution descriptors allowed to encode the proportion of important nodes (for a given node measure) and their level of importance inside the graph. Since the number of nodes per graph was 170 on average (see Section 2.2) the use of 10 percentiles, including the percentiles 0 and 100, allowed us to describe each distribution in a summarized form that still kept the shape of the distribution.

In order to see the effect of using this new morphology–based structure instead of a fixed structure, we used the same regional texture features and the

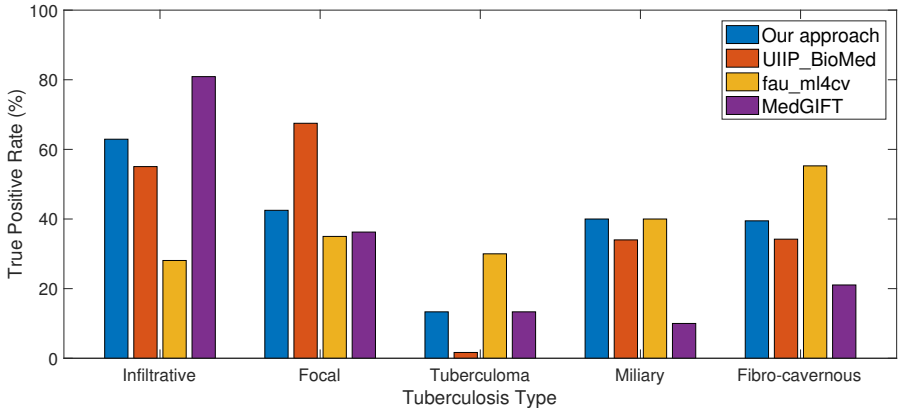

Fig. 7. True positive rate (%) for each TB type obtained by our approach and the top 3 groups participating in the ImageCLEF 2018 TB task.

same weight definition as Dicente *et al.* in [10]. The results, both in terms of accuracy and kappa value, clearly show the benefits of using our new graph structure (see Section 4) instead of the one used by the MedGIFT group, indicating that the global structure of the same texture information is as important as the local information.

The analysis of the confusion matrix shown in Figure 6 shows the strong effect produced by the unbalanced dataset. Patients with TB type 1 and 2 (T1 and T2) were much more frequent in the dataset than the other three TB types. This generated a bias in the classification of the test set towards these two classes since the optimization of our classifier was done using the overall cross–validation accuracy. Moreover, in the training phase we considered each CT scan as a different patient (see Section 3), therefore creating an even stronger effect towards classes T1 and T2 due to their higher proportion of scans (see Table 1). Analyzing the TPR for each TB type in Figure 7, the MedGIFT and UIIP_BioMed groups seem to have had a similar bias towards classes T1 and T2, but it is not the case for the fau_m4cv group that obtained a similar TPR for all the classes. In this task, the unweighted Cohen kappa coefficient is a better measure of the performance of the algorithms due to its invariance to unbalanced datasets. It indicates the level of agreement between the predicted labels and the ground truth labels considering their prior probability in the dataset, and therefore giving more importance to matches in rare classes than in frequent classes. All the results provided by the ImageCLEF organizers are reported in this work. Paired statistics between the algorithms could not be computed since individual results per patient were not available.

6 Conclusions

A new graph model of the lungs with a non–fixed morphology–based structure is proposed in this work for the classification of TB types in chest CT scans. We present a novel graph–based patient descriptor encoding the distributions inside the graph of five complementary node measures using percentiles. This technique allows us to characterize each patient graph in the same feature space, independently from the initial number of nodes and edges.

The evaluation in a public challenge strengthens the comparison of this new graph model against the other 39 participating algorithms, obtaining the top unweighted Cohen kappa coefficient and the second best overall classification accuracy. Although the obtained results are promising, better scores would be required to apply this model in medical practice. Nevertheless, the use of the same regional texture features and weight definition than in the graph model from the MedGIFT group shows the benefits of our new morphology–based structure. This confirms the importance of encoding the overall structure along the lung using similar tissue patterns.

Acknowledgments: This work was partly supported by the Swiss National Science Foundation in the PH4D project (grant agreement 320030–146804).

References

1. Achanta, R., Shaji, A., Smith, K., Lucchi, A., Fua, P., Süsstrunk, S.: SLIC superpixels compared to state–of–the–art superpixel methods. IEEE Transactions on Pattern Analysis and Machine Intelligence **34**(11), 2274–2282 (November 2012)
2. Andreu, J., Caceres, J., Pallisa, E., Martinez-Rodriguez, M.: Radiological manifestations of pulmonary tuberculosis. European journal of radiology **51**(2), 139–149 (2004)
3. Blumberg, H.M., Burman, W.J., Chaisson, R.E., Daley, C.L., et al.: American thoracic society/centers for disease control and prevention/infectious diseases society of america: treatment of tuberculosis. American journal of respiratory and critical care medicine **167**(4), 603 (2003)
4. Burrill, J., Williams, C.J., Bain, G., Conder, G., Hine, A.L., Misra, R.R.: Tuberculosis: a radiologic review. Radiographics **27**(5), 1255–1273 (2007)
5. Dicente Cid, Y., Batmanghelich, K., Müller, H.: Textured graph–based model of the lungs: Application on tuberculosis type classification and multi–drug resistance prediction. In: CLEF 2018. Springer LNCS (2018)
6. Dicente Cid, Y., Jimenez-del-Toro, O., Depeursinge, A., Müller, H.: Efficient and fully automatic segmentation of the lungs in CT volumes. In: Orcun Goksel, Jimenez-del-Toro, O., Foncubierta-Rodriguez, A., Müller, H. (eds.) Proceedings of the VISCERAL Challenge at ISBI. pp. 31–35. No. 1390 in CEUR Workshop Proceedings (Apr 2015)
7. Dicente Cid, Y., Jimenez-del-Toro, O., Platon, A., Müller, H., Poletti, P.A.: From local to global: A holistic lung graph model. In: Medical Image Computing and Computer–Assisted Intervention – MICCAI 2018 (2018)

8. Dicente Cid, Y., Kalinovsky, A., Liauchuk, V., Kovalev, V., , Müller, H.: Overview of ImageCLEFtuberculosis 2017 - predicting tuberculosis type and drug resistances. In: CLEF 2017 Labs Working Notes. CEUR Workshop Proceedings, CEUR-WS.org <http://ceur-ws.org>, Dublin, Ireland (September 11-14 2017)
9. Dicente Cid, Y., Liauchuk, V., Kovalev, V., , Müller, H.: Overview of ImageCLEFtuberculosis 2018 - detecting multi-drug resistance, classifying tuberculosis type, and assessing severity score. In: CLEF2018 Working Notes. CEUR Workshop Proceedings, CEUR-WS.org <http://ceur-ws.org>, Avignon, France (September 10-14 2018)
10. Dicente Cid, Y., Müller, H.: Texture-based graph model of the lungs for drug resistance detection, tuberculosis type classification, and severity scoring: Participation in ImageCLEF 2018 tuberculosis task. In: CLEF2018 Working Notes. CEUR Workshop Proceedings, CEUR-WS.org <http://ceur-ws.org>, Avignon, France (September 10-14 2018)
11. Dicente Cid, Y., Müller, H., Platon, A., Poletti, P.A., Depeursinge, A.: 3–D solid texture classification using locally–oriented wavelet transforms. IEEE Transactions on Image Processing **26**(4), 1899–1910 (April 2017)
12. Ishay, A., Marques, O.: Ensemble of 3D CNNs with multiple inputs for tuberculosis type classification. In: CLEF2018 Working Notes. CEUR Workshop Proceedings, CEUR-WS.org <http://ceur-ws.org>, Avignon, France (September 10-14 2018)
13. Liauchuk, V., Tarasau, A., Snezhko, E., Kovalev, V., Gabrielian, A., Rosenthal, A.: ImageCLEF 2018: Lesion-based TB-descriptor for CT image analysis. In: CLEF2018 Working Notes. CEUR Workshop Proceedings, CEUR-WS.org <http://ceur-ws.org>, Avignon, France (September 10-14 2018)
14. Liu, K., Skibbe, H., Schmidt, T., Blein, T., Palme, K., Brox, T., Ronneberger, O.: Rotation-invariant hog descriptors using fourier analysis in polar and spherical coordinates. International Journal of Computer Vision **106**(3), 342–364 (2014)
15. Parra, J.A.C., Zúñiga, N.M., Lara, C.S.: Tuberculosis the great imitator: False healing and subclinical activity. Indian Journal of Tuberculosis **64**(4), 345–348 (2017)
16. Richiardi, J., Bunke, H., Van De Ville, D., Achard, S.: Machine learning with brain graphs. IEEE Signal processing magazine **58** (2013)
17. Richiardi, J., Eryilmaz, H., Schwartz, S., Vuilleumier, P., Van De Ville, D.: Decoding brain states from fMRI connectivity graphs. NeuroImage **56**(2), 616–626 (2011). https://doi.org/10.1016/j.neuroimage.2010.05.081
18. Schabdach, J., Wells, W., Cho, M., Batmanghelich, K.N.: A likelihood-free approach for characterizing heterogeneous diseases in large-scale studies. In: International Conference on Information Processing in Medical Imaging. pp. 170–183. Springer (2017)
19. Sun, J., Chong, P., Tan, Y.X.M., Binder, A.: ImageCLEF 2017: ImageCLEF tuberculosis task - the SGEast submission. In: CLEF2017 Working Notes. CEUR Workshop Proceedings, CEUR-WS.org <http://ceur-ws.org>, Dublin, Ireland (September 11-14 2017)
20. Varoquaux, G., Gramfort, A., Poline, J., Thirion, B.: Brain covariance selection: better individual functional connectivity models using population prior. Nips **10**, 2334–2342 (2010)
21. World Health Organization, et al.: Global tuberculosis report 2016 (2016)